Magnetic properties of spin-1 Heisenberg antiferromagnet with easy-axis single-ion anisotropy in three dimensions: Linked-cluster series expansion approach

Kok-Kwei Pan

Physics Group, Center of General Education, Chang Gung University, No. 259, Wen-Hua 1st Road, Kwei-San, Tao-Yuan 33302, Taiwan, Republic of China

(Received 29 October 2008; revised manuscript received 19 February 2009; published 9 April 2009)

The magnetic properties of spin-1 Heisenberg and Ising antiferromagnet with easy-axis single-ion anisotropy are studied in both ordered phase and disordered phase by using the linked-cluster series expansion method. We calculate the seventh-order series for the free energy and staggered susceptibility and the sixth-order series for the staggered magnetization on three-dimensional bipartite lattices. We obtain accurate estimate of the Néel temperature, the critical exponent γ, and the staggered magnetization. The effect of quantum and thermal spin fluctuations on the magnetic ordering of the system is discussed.

DOI: 10.1103/PhysRevB.79.134414 PACS number(s): 75.10.Jm, 05.30.−d, 75.40.Cx

I. INTRODUCTION

In real magnetic materials with localized moments, single-ion anisotropy generated by crystal fields plays a major role in determining the magnetic behavior of the magnetic systems[1] with spin greater than 1/2. The low-dimensional anisotropic Heisenberg antiferromagnets have been intensively studied both theoretically and experimentally[2] for many years because of its possible relevance to the phenomenon of high-temperature superconductivity. In low-dimensional magnetic materials, single-ion anisotropy is important for establishing three-dimensional (3D) long-range order at a finite temperature and its influence has been included in analyses of the experimental data.[3]

There has been much theoretical work devoted over the years to investigate the magnetic properties of Heisenberg antiferromagnet with single-ion anisotropy on the linear chain and two-dimensional lattices by using various methods, including mean-field approximation (MFA),[4] exact diagonalization method,[5,6] Monte Carlo simulation method,[7,8] Green's-function approach,[5,9] spin-wave theory, and series expansion method at zero temperature.[10,11] However, systematic analytical studies of the model in three dimensions are quite rare, apart from recent theoretical studies using the coupled-cluster method[12] and bosonic mean-field theory.[13]

It is the purpose of this paper to study the magnetic properties of spin-1 Heisenberg antiferromagnet (HAF) with easy-axis single-ion anisotropy for the simple cubic (sc) lattice and the body-centered-cubic (bcc) lattice by using linked-cluster series expansion method. This method has been extensively used on the spin-$\frac{1}{2}$ quantum Heisenberg antiferromagnet[14] and ferromagnetic spin systems.[15,16] The method sums up all perturbation terms to a certain order and estimates the result through a well-developed extrapolation method. The accurate results for thermodynamic quantities of the magnetic systems are obtained both in the ordered phase and disordered phase. In the disordered phase the linked-cluster series are identical to the high-temperature series. In the ordered phase, correlations of spin and thermal fluctuations are included in the perturbation expansion and the order parameter is found self-consistently from the series of the staggered magnetization.

The Hamiltonian of spin-1 anisotropic Heisenberg antiferromagnet with easy-axis single-ion anisotropy is given by

$$H = J\sum_{\langle i,j\rangle}[S_i^z S_j^z + \lambda(S_i^x S_j^x + S_i^y S_j^y)] - D\sum_j (S_j^z)^2 - h_s\sum_{i\in A} S_i^z + h_s\sum_{j\in B} S_j^z, \quad (1)$$

where the antiferromagnetic pair exchange interaction ($J>0$) is restricted to nearest neighbors and λ is the anisotropy of the exchange interaction varying between 0 and 1. D is a positive parameter and measures the strength of the single-ion anisotropy. The single-ion anisotropy in the Hamiltonian [Eq. (1)] forces the spins to lie along the z axis and the system will order along the z axis, namely, the easy axis. h_s in the Zeeman energy term is staggered magnetic fields on two sublattices A and B for calculating the staggered susceptibility. The lattice has been divided into two distinct interpenetrating sublattices.

We have obtained the exact seventh-order series for the free energy and staggered susceptibility and the sixth-order series for the staggered magnetization on three-dimensional bipartite lattices. The series are analyzed using the standard ratio and Padé approximant techniques.[17]

A brief outline of the paper is as follows. The linked-cluster series expansion method which treats the single-ion anisotropy exactly is presented in Sec. II. Analysis of the series and the results of the calculation are presented in Sec. III. A summary and conclusions is given in Sec. IV.

II. LINKED-CLUSTER SERIES EXPANSION

The Hamiltonian is divided into an unperturbed mean-field Hamiltonian H_0 and a perturbation part H_1, i.e.,

$$H = H_0 + H_1. \quad (2)$$

The mean-field Hamiltonian H_0 includes all single-ion potentials and a self-consistent field term extracted from the pair exchange interaction potential,

TABLE I. List of free-energy connected diagrams, the corresponding weight factors, and lattice constants through sixth order.

Graph	Weight	Lattice Constant
	2	LC(1)
	1	LC(1)
	4	LC(1)
	6	LC(1)
	8	LC(1)
	24	LC(1)
	3	LC(1)
	48	LC(2)
	48	LC(2)
	12	LC(2)
	48	LC(4)
	6	LC(4)
	16	LC(1)
	80	LC(1)
	30	LC(1)
	320	LC(2)
	160	LC(2)
	480	LC(2)
	240	LC(2)
	960	LC(4)
	480	LC(4)
	240	LC(4)
	32	LC(1)
	240	LC(1)

Graph	Weight	Lattice Constant
	180	LC(1)
	10	LC(1)
	960	LC(2)
	2880	LC(2)
	480	LC(2)
	360	LC(2)
	1440	LC(2)
	180	LC(2)
	640	LC(2)
	1920	LC(2)
	1440	LC(2)
	960	LC(3)
	1440	LC(3)
	720	LC(3)
	120	LC(3)
	2880	LC(3)
	2880	LC(3)
	1440	LC(3)
	1440	LC(3)
	720	LC(3)
	360	LC(3)

Graph	Weight	Lattice Constant
	3840	LC(4)
	5760	LC(4)
	1440	LC(4)
	360	LC(4)
	2880	LC(4)
	2880	LC(4)
	720	LC(4)
	1440	LC(4)
	5760	LC(4)
	5760	LC(4)
	1440	LC(4)
	2880	LC(4)
	11520	LC(5)
	5760	LC(5)
	1440	LC(5)
	720	LC(5)
	3840	LC(6)
	1440	LC(6)
	3840	LC(7)
	120	LC(7)

$$H_0 = \sum_{i \in A} \{-D(S_i^z)^2 - [JzM^+ + h_s]S_i^z\} + \sum_{j \in B} \{-D(S_i^z)^2 + [JzM^+ + h_s]S_j^z\} + \frac{1}{2}NJz(M^+)^2, \quad (3)$$

where z is the number of nearest neighbors and N is the total number of sites in a lattice. M^+ is the staggered magnetization which minimizes the free energy of the system.

The perturbation Hamiltonian H_1 includes the effects of thermal and quantum fluctuation correlations as follows:

$$H_1 = J\sum_{\langle i,j \rangle} [S_i^z - M^+][S_j^z + M^+] + \frac{J\lambda}{2}\sum_{\langle i,j \rangle} [S_i^+ S_j^- + S_i^- S_j^+]. \quad (4)$$

Generally, the mean-field Hamiltonian is used to study the thermodynamic quantities for such system because of the complexities caused by the single-ion anisotropy terms.

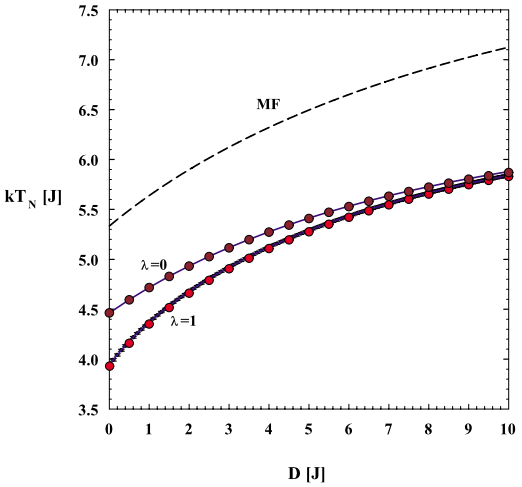

FIG. 1. (Color online) Néel temperature kT_N/J as a function of easy-axis anisotropy D/J for Ising antiferromagnet ($\lambda=0$) and isotropic Heisenberg antiferromagnet ($\lambda=1$) for the bcc lattice. Solid line is the results of the linked-cluster series by using the ratio method. The filled circles are the results of D-logarithmic Padé approximants, with estimated errors no larger than the size of the symbols. The dashed line is the mean-field results.

However, both quantum and thermal spin fluctuation correlations have been neglected in the mean-field Hamiltonian. The mean-field system consists of a single-spin excited $S^z=0$ state separated from its ordered $S^z=\pm 1$ states by an energy gap of D due to the single-ion anisotropy. In terms of eigenstates and eigenvalues of the S^z operator, the eigenstates for local site of the mean-field Hamiltonian H_0 are $|\epsilon_1\rangle=|1\rangle$, $|\epsilon_2\rangle=|0\rangle$, and $|\epsilon_3\rangle=|-1\rangle$ and the corresponding eigenenergies for sublattices A and B are

$$\epsilon_1^A = -D - [JzM^+ + h_s] + \epsilon_0, \quad \epsilon_1^B = -D + [JzM^+ + h_s] + \epsilon_0,$$

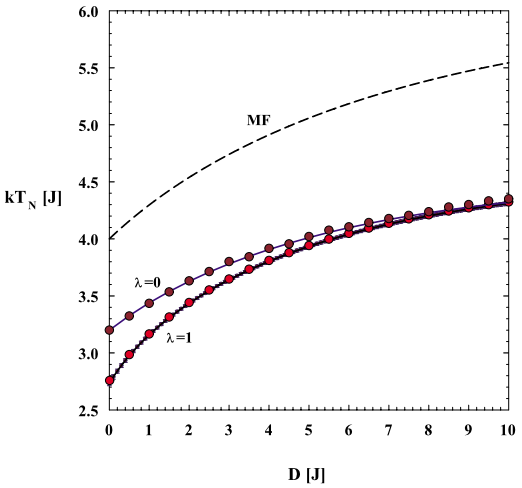

FIG. 2. (Color online) Néel temperature kT_N/J as a function of easy-axis anisotropy D/J for Ising antiferromagnet ($\lambda=0$) and isotropic Heisenberg antiferromagnet ($\lambda=1$) for the sc lattice. Solid line is the results of the linked-cluster series by using the ratio method. The filled circles are the results of D-logarithmic Padé approximants, with estimated errors no larger than the size of the symbols. The dashed line is the mean-field results.

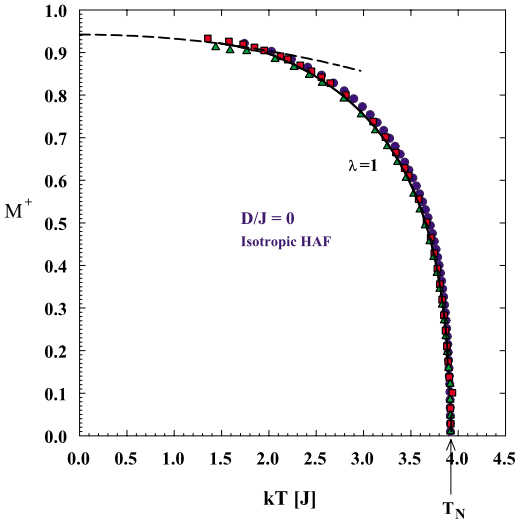

FIG. 3. (Color online) Staggered magnetization M^+ as a function of temperature kT/J of spin-1 isotropic HAF model ($D/J=0$) for the bcc lattice. Solid line is the series results obtained from the ratio method. The results obtained from $[\frac{2}{2}]$ (open circle), $[\frac{3}{2}]$ (square), and $[\frac{2}{3}]$ (triangle) Padé approximants are also shown. Dashed line is the predictions of spin-wave theory. T_N indicates the estimate of Néel temperature from high-temperature series.

$$\epsilon_2^A = \epsilon_0, \quad \epsilon_2^B = \epsilon_0,$$

$$\epsilon_3^A = -D + [JzM^+ + h_s] + \epsilon_0, \quad \epsilon_3^B = -D - [JzM^+ + h_s] + \epsilon_0, \tag{5}$$

where $\epsilon_0=\frac{1}{2}NJz(M^+)^2$.

The mean-field free energy per site F_0 is

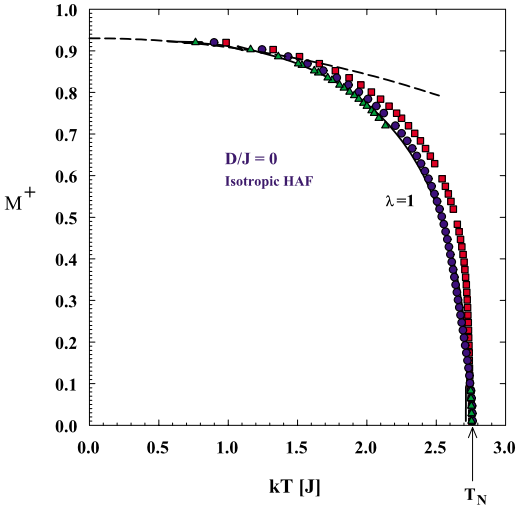

FIG. 4. (Color online) Staggered magnetization M^+ as a function of temperature kT/J of spin-1 isotropic HAF model ($D/J=0$) for the sc lattice. Solid line is the series results obtained from the ratio method. The results obtained from $[\frac{2}{2}]$ (open circle), $[\frac{3}{2}]$ (square), and $[\frac{2}{3}]$ (triangle) Padé approximants are also shown. Dashed line is the predictions of spin-wave theory. T_N indicates the estimate of Néel temperature from high-temperature series.

TABLE II. The nonzero lattice constants (LCs) in terms of weak embedded lattice constants for the bipartite lattices.

LC number	LC in terms of weak embedded lattice constant
LC(1)	z
LC(2)	z^2
LC(3)	z^3
LC(4)	$8p_4+2z^2-z$
LC(5)	$8zp_4+2z^3-z^2$
LC(6)	$12p_{6A}+24p_4+z^3+z^2-z$
LC(7)	$12p_6-48p_4+48zp_4+5z^3-6z^2+2z$

$$F_0 = -\frac{1}{\beta}\{\ln[1+2e^x\cosh(y_0)]\}, \tag{6}$$

where $x=\beta D$, $y_0=\beta\{JzM_0^+ + h_s\}$, and $\beta=(k_BT)^{-1}$. The mean-field staggered magnetization per site M_0^+ is obtained from the free energy by taking a derivative with respect to h_s,

$$M_0^+ = -\frac{\partial F_0}{\partial h_s} = \frac{2e^x\sinh(y_0)}{1+2e^x\cosh(y_0)}, \tag{7}$$

where $y_0=\beta\{JzM_0^+ + h_s\}$.

In order to incorporate the quantum and thermal fluctuation correlations due to H_1, we now apply the linked-cluster series expansion as follows. The free energy F can be written as

$$F = F_0 + \Delta F, \tag{8}$$

where F_0 is the free-energy term corresponding to the mean-field Hamiltonian H_0. ΔF, the corrections of free energy to F_0 due to the quantum and thermal fluctuation correlations, is expressed as[18]

$$\Delta F = -\frac{1}{\beta}\sum_{n=1}^{\infty}\frac{(-1)^n}{n!}\int_0^\beta \times d\tau_1\int_0^\beta d\tau_2\cdots\int_0^\beta d\tau_n\langle T_\tau[H_1(\tau_1)H_1(\tau_2)\cdots H_1(\tau_n)]\rangle_c, \tag{9}$$

where $\beta=(k_BT)^{-1}$. Operators in Eq. (9) are written in the interaction picture, and the subscript c denotes the cumulant part of the τ-ordered product or, in the diagram analysis, the contribution of the connected diagrams.

It is convenient to represent the terms in the series expansion of free energy ΔF by diagrams. A product of $H_1(\tau)$ in the free-energy expansion is represented by diagrams which are composed of lines and arrows. A line denotes a longitudinal interaction $[S_i^z-M^+][S_j^z+M^+]$ and a solid line with an arrow represents a transverse interaction $S_i^+S_j^-$. The expansion of ΔF then can be expressed as

$$\Delta F = -\frac{1}{\beta}\sum_{n,g_n}^{\infty}\frac{(-1)^n}{n!}W(g_n)L(g_n)I(g_n). \tag{10}$$

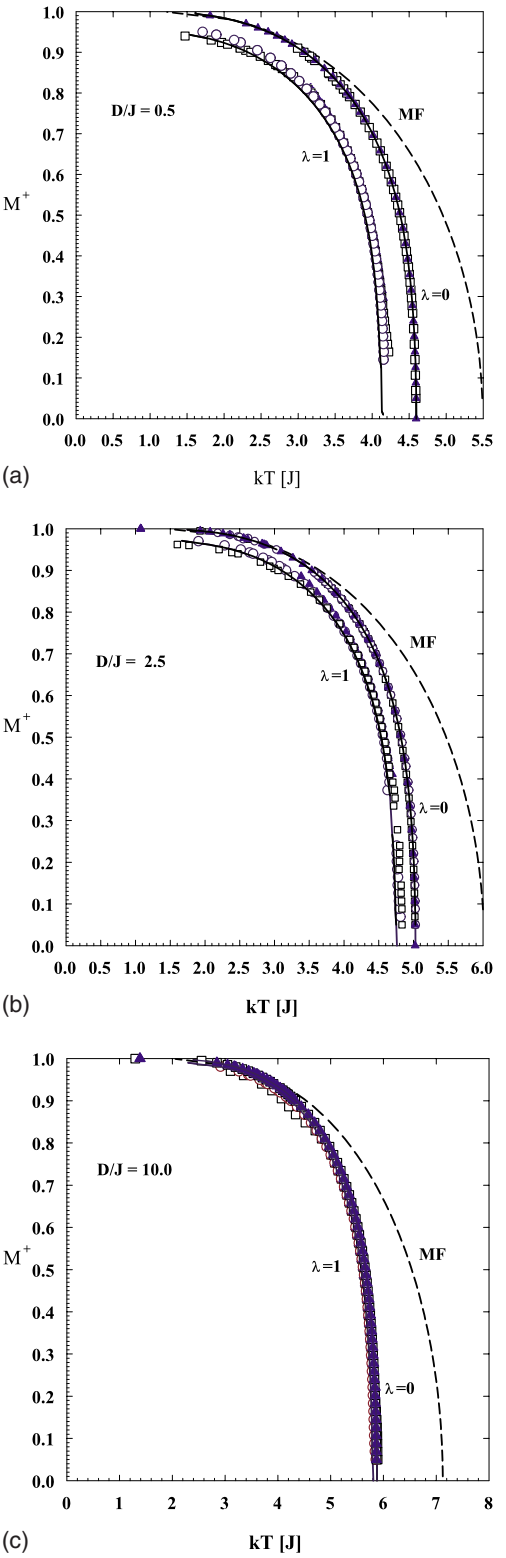

FIG. 5. (Color online) Staggered magnetization M^+ as a function of temperature kT/J of spin-1 Ising antiferromagnet ($\lambda=0$) and isotropic Heisenberg antiferromagnet ($\lambda=1$) with easy-axis anisotropy for the bcc lattice: (a) $D/J=0.5$, (b) $D/J=2.5$, and (c) $D/J=10.0$. Solid line is the series results obtained from the ratio method. The results obtained from $[\frac{2}{2}]$ (open circle), $[\frac{3}{2}]$ (square), and $[\frac{2}{3}]$ (triangle) Padé approximants are also shown. The dashed line is the mean-field results.

The summation is over all linked (connected) diagrams where g_n indicates an nth-order linked diagram. $W(g_n)$ is the weight of the diagram or the number of topologically equivalent diagrams that appear in the expansion. $L(g_n)$ is the *lattice constant* of the diagram. $I(g_n)$ is the value of the τ integral of the cumulant product which the diagram represents. Summation over the lattice sites is obtained by taking the appropriate free multiplicity as the lattice constant[19] and multiplying the term by J^n. In Table I we show all diagrams, the corresponding weight factors, and lattice constants through sixth order. The corresponding lattice constants in terms of weak embedded lattice constants[20] for the bipartite lattices are shown in Table II. Seventh-order diagrams are available upon request.

The first step in the calculation of the τ integrals implied by each diagram in Table I is to express the cumulants or the semi-invariants in terms of moments or thermal averages. We use Eq. (11) to transform the cumulants to the moments,[21] where $\langle T_\tau[S_1 S_2 \cdots S_n]\rangle_c$ represents the cumulant of the product of spin operators,

$$\langle T_\tau[S_1(\tau_1)S_2(\tau_2)\cdots S_n(\tau_n)]\rangle_c = \sum_{l=1}^{n} (l-1)\,!\,(-1)^{l-1} \sum_{p(n,l)} \left\langle T_\tau\left[\prod_{j=1}^{m_1} S_j(\tau_j)\right]\right\rangle_0 \cdots \left\langle T_\tau\left[\prod_{q=1}^{m_k} S_q(\tau_q)\right]\right\rangle_0 . \tag{11}$$

$p(n,l)$ represents a partition of n operators $S_1, S_2, \ldots, S_n$ into l sets without regard to the order and $m_1, m_2, \ldots, m_k$ represents the number of operators in each set. A program has been developed to calculate this transformation.

The calculation of the multiple integrals containing τ-ordered products of spin operators of Eq. (9) for quantum spin models with single-ion anisotropy is complicated because of noncommutativity of the spin operators. We use the following standard basis operators in order to facilitate the calculation of the multiple integrals containing τ-ordered products of spin operators in series expansion:

$$L_{mn} \equiv |\epsilon_m\rangle\langle\epsilon_n|, \quad m,n = 1,2,3, \tag{12}$$

where $|\epsilon_m\rangle$ and $|\epsilon_n\rangle$ are eigenstates of mean-field Hamiltonian H_0. These operators satisfy the following multiplication rule and commutation relation:[15,16]

$$L^i_{\alpha\beta} L^i_{\gamma\eta} = \delta_{\beta\gamma} L^i_{\alpha\eta}, \tag{13}$$

$$[L^i_{\alpha\beta}, L^j_{\gamma\eta}] = \delta_{ij}(\delta_{\beta\gamma} L^i_{\alpha\eta} - \delta_{\eta\alpha} L^i_{\gamma\beta}), \tag{14}$$

where $i,j,\ldots$ are the labels of the lattice sites. The standard basis operators in the interaction picture have the simple τ dependence,

$$L_{mn}(\tau) = e^{(\epsilon_m - \epsilon_n)\tau} L_{mn}(0). \tag{15}$$

The spin operators[22] are rewritten in terms of the standard basis operators as

$$S^+ = \sqrt{2}(L_{12} + L_{23}),$$

$$S^- = \sqrt{2}(L_{21} + L_{32}),$$

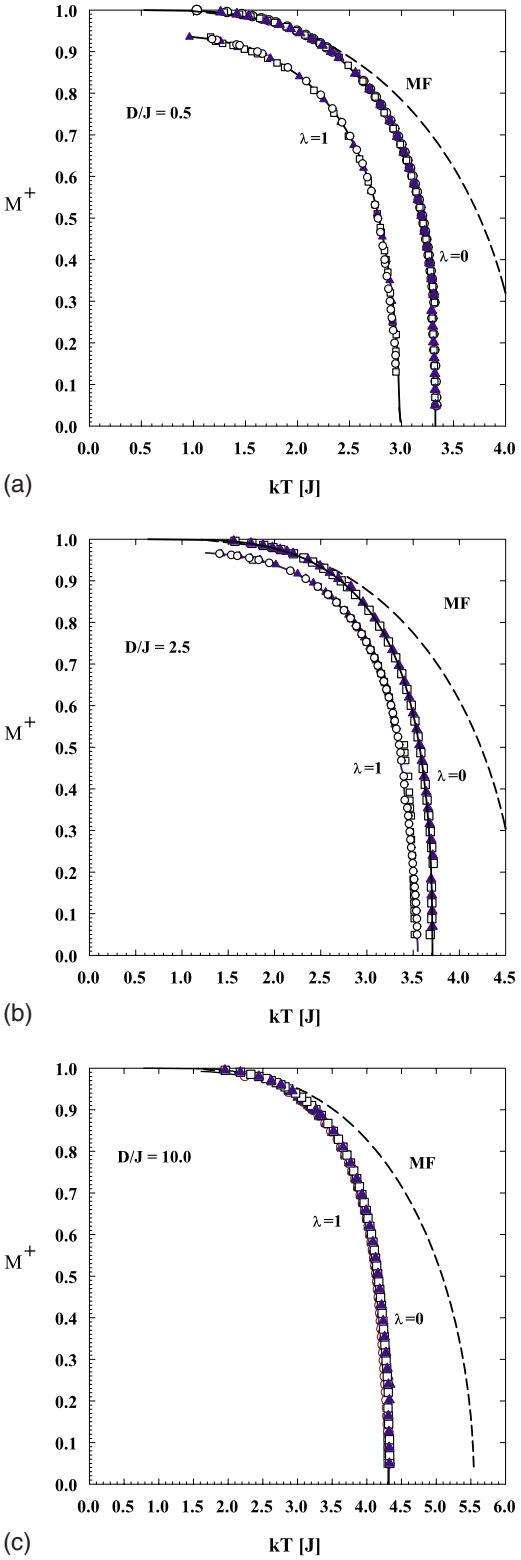

FIG. 6. (Color online) Staggered magnetization M^+ as a function of temperature kT/J of spin-1 Ising antiferromagnet ($\lambda=0$) and isotropic Heisenberg antiferromagnet ($\lambda=1$) with easy-axis anisotropy for the sc lattice: (a) $D/J=0.5$, (b) $D/J=2.5$, and (c) $D/J=10.0$. Solid line is the series results obtained from the ratio method. The results obtained from $[\frac{2}{2}]$ (open circle), $[\frac{3}{2}]$ (square), and $[\frac{2}{3}]$ (triangle) Padé approximants are also shown. The dashed line is the mean-field results.

$$S^z = (L_{11} - L_{33}). \tag{16}$$

The replacement of the product of spin operators by standard basis operators in the thermal average expression is also done by a computer program.

The evaluation of multiple τ-ordered integrals has been a major obstacle in obtaining long series for quantum spin systems. Numerous algebras must be done to evaluate the multiple integrals for the higher-order terms. We use the multiple-site Wick reduction theorem[15,16] to calculate the multiple integrals. A product of the same τ standard basis operators in the integrand is replaced with an operator O_k defined as

$$O_k(\tau_k) = L^i_{\alpha\beta}(\tau_k) L^j_{\gamma\delta}(\tau_k) \cdots . \tag{17}$$

Therefore, the multiple integral now contains products of the O operators defined in Eq. (17). The integrals containing a product of the O operators are then calculated by using the multiple-site Wick reduction theorem,

$$\begin{aligned}
&\int_0^\beta d\tau_1 \cdots \int_0^\beta d\tau_k \cdots \int_0^\beta d\tau_n \langle T_\tau [O_1(\tau_1) \cdots O_k(\tau_k) \cdots O_n(\tau_n)] \rangle_0 \\
&= \frac{1}{\epsilon_k} \int_0^\beta d\tau_1 \cdots \int_0^\beta d\tau_n [\langle T_\tau \{[O_1, O_k]_{\tau_1} \cdots O_n(\tau_n)\} \rangle_0 \\
&\quad + \langle T_\tau \{O_1(\tau_1)[O_2, O_k]_{\tau_2} \cdots O_n(\tau_n)\} \rangle_0 + \cdots \\
&\quad + \langle T_\tau \{O_1(\tau_1) \cdots [O_n, O_k]_{\tau_n}\} \rangle_0],
\end{aligned} \tag{18}$$

where ϵ_k is the energy associated with the operator $O_k(\tau_k)$ defined by

$$\epsilon_k = (E_{\alpha_k} - E_{\beta_k}) + (E_{\gamma_k} - E_{\delta_k}) + \cdots . \tag{19}$$

An n-fold integral is thus reduced to a sum of $(n-1)$-fold integrals. The mixture of τ-dependent O operators integrals can be calculated by successive application of Eq. (18). τ-independent O operators integrals are calculated by forming all permutations of the operators and multiplying the results by the factor $\beta^n/n!$, where n is the number of O operators in the integrand. A computer program has been developed to perform τ-dependent integral as well as τ-independent integral calculation symbolically.

The multiple-site Wick integration procedure is demonstrated on the following integral which is generated from the third-order diagram with two transverse and one longitudinal interaction lines:

$$\begin{aligned}
I = \int_0^\beta d\tau_1 \int_0^\beta d\tau_2 \int_0^\beta d\tau_3 \langle T_\tau \{L^1_{23}(\tau_1) L^1_{32}(\tau_2) [L^1_{11} - L^1_{33} - M^+] \\
\times (\tau_3)\} \rangle_0 \langle T_\tau \{L^2_{21}(\tau_1) L^2_{12}(\tau_2) [L^2_{11} - L^2_{33} + M^+](\tau_3)\} \rangle_0,
\end{aligned} \tag{20}$$

where the superscripts 1 and 2 of the operators are defined to be the labels for sublattices A and B, respectively. Operators with the same τ are grouped together and the site labels are replaced with A and B,

$$\begin{aligned}
I = \int_0^\beta d\tau_1 \int_0^\beta d\tau_2 \int_0^\beta d\tau_3 \langle T_\tau \{ \underbrace{L^A_{23}(\tau_1) L^B_{21}(\tau_1)}_{O_1(\tau_1)} \underbrace{L^A_{32}(\tau_2) L^B_{12}(\tau_2)}_{O_2(\tau_2)} \\
\times \underbrace{[L^A_{11} - L^A_{33} - M^+](\tau_3)[L^B_{11} - L^B_{33} + M^+](\tau_3)}_{O_3(\tau_3)} \} \rangle_0 .
\end{aligned} \tag{21}$$

The first operator O_1 in the product of Eq. (21) is chosen to be active operator O_k in Eq. (18). Application of the multiple-site Wick integral formula and commutation relation yields

$$\begin{aligned}
I = \frac{1}{2\{D - (JzM^+ + h_s)\}} \Bigg\{ &+ \int_0^\beta d\tau_2 \int_0^\beta d\tau_3 \langle T_\tau \{ \underbrace{L^A_{33}(\tau_2) L^B_{11}(\tau_2)}_{O_2(\tau_2)} \underbrace{[L^A_{11} - L^A_{33} - M^+](\tau_3)[L^B_{11} - L^B_{33} + M^+](\tau_3)}_{O_3(\tau_3)} \} \rangle_0 \\
&- \int_0^\beta d\tau_2 \int_0^\beta d\tau_3 \langle T_\tau \{ \underbrace{L^A_{22}(\tau_2) L^B_{22}(\tau_2)}_{O_2(\tau_2)} \underbrace{[L^A_{11} - L^A_{33} - M^+](\tau_3)[L^B_{11} - L^B_{33} + M^+](\tau_3)}_{O_3(\tau_3)} \} \rangle_0 \\
&- (M^+)^2 \int_0^\beta d\tau_2 \int_0^\beta d\tau_3 \langle T_\tau \{ \underbrace{L^A_{32}(\tau_2) L^B_{12}(\tau_2)}_{O_2(\tau_2)} \underbrace{L^A_{23}(\tau_3) L^B_{21}(\tau_3)}_{O_3(\tau_3)} \} \rangle_0 \\
&+ (1 + M^+)^2 \int_0^\beta d\tau_2 \int_0^\beta d\tau_3 \langle T_\tau \{ \underbrace{L^A_{32}(\tau_2) L^B_{12}(\tau_2)}_{O_2(\tau_2)} \underbrace{L^A_{23}(\tau_3) L^B_{21}(\tau_3)}_{O_3(\tau_3)} \} \rangle_0 \Bigg\}.
\end{aligned} \tag{22}$$

The first and second integrals in Eq. (22) are τ independent and can be calculated by the method described earlier. The third and fourth integrals can be calculated by applying the multiple-site Wick reduction theorem again. The value of I is obtained as

$$I = -\frac{1}{2}\frac{\beta^2}{\{D-(JzM^+ + h_s)\}}(1+M^+)^2\langle L_{33}^A\rangle_0\langle L_{11}^B\rangle_0 + \frac{1}{2}\frac{\beta^2}{\{D-(JzM^+ + h_s)\}}(M^+)^2\langle L_{22}^A\rangle_0\langle L_{22}^B\rangle_0 + \frac{1}{4}\frac{\beta}{\{D-(JzM^+ + h_s)\}^2}(M^+)^2\{\langle L_{22}^A\rangle_0\langle L_{22}^B\rangle_0 - \langle L_{33}^A\rangle_0\langle L_{11}^B\rangle_0\} - \frac{1}{4}\frac{\beta}{\{D-(JzM^+ + h_s)\}^2}(1+M^+)^2\{\langle L_{22}^A\rangle_0\langle L_{22}^B\rangle_0 - \langle L_{33}^A\rangle_0\langle L_{11}^B\rangle_0\}.$$

The thermal averages of standard basis operators for sublattices A and B are calculated as

$$\langle L_{11}^A\rangle_0 = \frac{e^{x+y}}{1+e^{x+y}+e^{x-y}}, \quad \langle L_{11}^B\rangle_0 = \frac{e^{x-y}}{1+e^{x+y}+e^{x-y}},$$

$$\langle L_{22}^A\rangle_0 = \frac{1}{1+e^{x+y}+e^{x-y}}, \quad \langle L_{22}^B\rangle_0 = \frac{1}{1+e^{x+y}+e^{x-y}},$$

$$\langle L_{33}^A\rangle_0 = \frac{e^{x-y}}{1+e^{x+y}+e^{x-y}}, \quad \langle L_{33}^B\rangle_0 = \frac{e^{x+y}}{1+e^{x+y}+e^{x-y}}. \quad (23)$$

The free-energy series per site F of the system calculated by the method described above is obtained as

$$F = F_0 + \sum_{n=2}^{\infty} f_n(x,y,\lambda)(\beta J)^n, \quad (24)$$

where f_n is a polynomial in the functions $x=\beta D$, λ, and $y=\beta\{JzM^+ + h_s\}$. We have obtained the first eight coefficients in the free-energy series.

Differentiating the free-energy series with respect to h_s, we obtain the staggered magnetization series M^+,

$$M^+ = -\frac{\partial F}{\partial h_s} = \frac{\partial(\beta F)}{\partial y} = M_0^+ + \sum_{n=2}^{\infty} m_n(x,y,\lambda)\{\beta J\}^n. \quad (25)$$

We obtained the staggered magnetization series up to sixth order.

The staggered susceptibility series is calculated from the staggered magnetization series by

$$\chi^s = \beta\frac{\partial M^+}{\partial y} \Big/ \left[1 - \beta J z\frac{\partial M^+}{\partial y}\right]. \quad (26)$$

In the disordered phase, zero-field ($h_s=0$) staggered susceptibility series is given as

TABLE III. Estimates of Néel temperatures kT_N/J by D-logarithmic Padé approximants. Poles of D-logarithmic Padé approximants to the staggered susceptibility series are listed with different values of easy-axis anisotropy D/J for the bcc lattice.

D/J	M/L	2	3	4
	2	4.331	4.347	4.462
1.0	3	4.352	4.270	
	4	4.375		
	2	4.639	4.655	4.787
2.0	3	4.661	4.539	
	4	4.685		
	2	4.885	4.900	5.036
3.0	3	4.906	4.778	
	4	4.928		
	2	5.089	5.103	5.232
4.0	3	5.109	4.996	
	4	5.129		
	2	5.260	5.272	5.402
5.0	3	5.276	5.184	
	4	5.294		
	2	5.406	5.417	5.542
6.0	3	5.420	5.345	
	4	5.437		
	2	5.532	5.542	5.662
7.0	3	5.545	5.484	
	4	5.560		
	2	5.641	5.651	5.764
8.0	3	5.653	5.603	
	4	5.667		
	2	5.736	5.745	5.852
9.0	3	5.747	5.706	
	4	5.760		
	2	5.819	5.827	5.928
10.0	3	5.829	5.794	
	4	5.841		

$$\beta^{-1}\chi^s = \sum_{n=0}^{\infty} a_n(x,\lambda)\{\beta J\}^n. \quad (27)$$

The coefficients of m_n and a_n are too long to be presented here. The full expressions of the staggered magnetization

series and the staggered susceptibility series expansion are available upon request.

The series obtained have been checked in the $D=0$ limit. In the $D=0$ limit and $\lambda=1$, the coefficients of our zero-field ($h_s=0$) staggered susceptibility series up to seventh order are identical to those of the high-temperature series[22,23] found for the isotropic Heisenberg antiferromagnetic model. In the $D=0$ and Ising $\lambda=0$ limits, the results of the current calculation in the paramagnetic phase ($T>T_N$) agree with previous results.[17]

III. ANALYSIS OF THE SERIES

A. Phase boundary: $T>T_N$

The transition between longitudinally ordered phase and the paramagnetic phase can be obtained by looking at the divergence of the paramagnetic staggered susceptibility series. For each value of D/J, the Néel temperature kT_N/J is estimated from the strong singularity in the paramagnetic staggered susceptibility series [Eq. (27)] by using the ratio method.[17]

For each value of D/J, kT_N/J is estimated self-consistently from the extrapolation given by

$$\frac{kT_N}{J}=\mu(n,m)=\frac{1}{n-m}[n\nu_n-m\nu_m], \tag{28}$$

where $\nu_n=a_n(x)/a_{n-1}(x)$. In Figs. 1 and 2 we show the second-order phase boundary Néel temperature kT_N/J as a function of single-ion anisotropy D/J for Ising antiferromagnet ($\lambda=0$) and isotropic Heisenberg antiferromagnet ($\lambda=1$) obtained from the ratio method for the bcc lattice and the sc lattice, respectively. They are plotted as a solid line which is estimated from the average of the seventh-order $\mu(7,5)$ and the sixth-order $\mu(6,4)$ extrapolations. The extrapolation shows good convergence in the sense that each extrapolation value differs from the average value by less than 1%. We have also performed D-logarithmic Padé approximants of the staggered susceptibility series [Eq. (27)] to obtain the Néel temperature. In Tables III and IV we list the poles of D-logarithmic Padé approximants to the staggered susceptibility series of isotropic Heisenberg antiferromagnetic model for the sc lattice and the bcc lattice, respectively. The second-order phase boundary kT_N/J vs D/J obtained from the average of $[\frac{2}{2}]$, $[\frac{2}{3}]$, $[\frac{2}{4}]$, $[\frac{3}{2}]$, $[\frac{3}{3}]$, and $[\frac{4}{2}]$ Padé approximants is also plotted in Figs. 1 and 2. It is clear from Figs. 1 and 2 that the results of D-logarithmic Padé approximants analysis are consistent with those obtained from the ratio method. The mean-field results are also plotted (dashed line) for comparison in Figs. 1 and 2.

The transverse spin fluctuation correlation, included in the perturbation, is controlled by the anisotropy parameter λ. The spin-1 systems with $\lambda=0$ and $\lambda=1$, which correspond to the spin-1 Ising antiferromagnetic model and isotropic Heisenberg antiferromagnetic model, have antiferromagnetic long-range order below the Néel critical temperature. Since the easy-axis anisotropy D favors the Néel order, the critical temperature kT_N/J increases as D/J increases. The spin fluctuations arising from the transverse exchange interaction tends to destroy the Néel ordered spins by creating $S^z=0$ state on neighboring sites and spreading the spin fluctuations through the entire lattice and thus reduce the Néel critical temperature. For the small energy gap D, where the transverse spin fluctuation correlation term is dominant, we see that the critical temperature of isotropic Heisenberg antiferromagnetic system is substantially reduced from that of the

TABLE IV. Estimates of Néel temperatures kT_N/J by D-logarithmic Padé approximants. Poles of D-logarithmic Padé approximants to the staggered susceptibility series are listed with different values of easy-axis anisotropy D/J for the sc lattice.

D/J	M/L	2	3	4
	2	3.165	3.172	3.165
1.0	3	3.171	3.167	
	4	3.155		
	2	3.440	3.447	3.441
2.0	3	3.446	3.442	
	4	3.433		
	2	3.647	3.652	3.647
3.0	3	3.651	3.648	
	4	3.638		
	2	3.812	3.813	3.811
4.0	3	3.813	3.812	
	4	3.800		
	2	3.944	3.944	3.943
5.0	3	3.944	3.944	
	4	3.930		
	2	4.053	4.051	4.052
6.0	3	4.051	4.053	
	4	4.215		
	2	4.142	4.140	4.142
7.0	3	4.139	4.143	
	4	4.125		
	2	4.216	4.213	4.216
8.0	3	4.217	4.217	
	4	4.197		
	2	4.277	4.273	4.278
9.0	3	4.272	4.279	
	4	4.257		
	2	4.327	4.323	4.329
10.0	3	4.322	4.331	
	4	4.306		

TABLE V. Estimates of critical exponent γ's from the Padé approximant to $-(\beta J-\beta_N J)[d/d(\beta J)]\ln \chi^s$ at the critical point $\beta_N J=J/(kT_N)$ for the bcc lattice.

D/J	kT_N/J	M/L	2	3	4	5
		2	1.321	1.319	1.317	1.311
1.0	4.351	3	1.319	1.320	1.306	
		4	1.319	1.203		
		5	1.313			
		2	1.285	1.283	1.281	1.276
2.0	4.660	3	1.283	1.285	1.271	
		4	1.283	1.252		
		5	1.277			
		2	1.268	1.266	1.265	1.261
3.0	4.905	3	1.266	1.267	1.259	
		4	1.266	1.253		
		5	1.262			
		2	1.258	1.256	1.255	1.252
4.0	5.107	3	1.256	1.257	1.251	
		4	1.256	1.248		
		5	1.252			
		2	1.255	1.254	1.253	1.251
5.0	5.275	3	1.254	1.254	1.251	
		4	1.253	1.249		
		5	1.251			
		2	1.252	1.251	1.251	1.250
6.0	5.420	3	1.251	1.252	1.249	
		4	1.251	1.249		
		5	1.250			
		2	1.251	1.250	1.250	1.249
7.0	5.545	3	1.250	1.251	1.249	
		4	1.250	1.248		
		5	1.249			
		2	1.261	1.262	1.258	1.261
8.0	5.643	3	1.261	1.259	1.260	
		4	1.259	1.260		
		5	1.260			
		2	1.259	1.260	1.257	1.259
9.0	5.739	3	1.259	1.258	1.259	
		4	1.258	1.259		
		5	1.259			
		2	1.258	1.259	1.256	1.258
10.0	5.822	3	1.258	1.257	1.258	
		4	1.257	1.258		
		5	1.258			

Ising system. For large D, the ordered ground $S^z=\pm 1$ states are isolated from the excited $S^z=0$ state and thus the disordering effect of spin fluctuations is suppressed. Accordingly, the Heisenberg antiferromagnetic system shows Ising-type antiferromagnetic critical behavior. In the limit $D\rightarrow+\infty$, the properties of the model approach those of the spin-1 antiferromagnetic Ising model.

B. Critical exponent γ estimates

The critical exponent for susceptibility γ is estimated from the D-logarithmic Padé approximants to the paramagnetic staggered susceptibility series by evaluating the equation[24]

$$\gamma=-(\beta J-\beta_N J)\frac{d\ln\chi^s(\beta J)}{d(\beta J)} \tag{29}$$

at the critical point $\beta_N J=J/(kT_N)$. Using the Néel temperature obtained from Sec. III A, we show the Padé approximant analysis of the series [Eq. (29)] for isotropic Heisenberg antiferromagnetic model ($\lambda=1$) with different values of easy-axis anisotropy D/J in Tables V and VI for the bcc lattice and the sc lattice, respectively. For the bcc lattice, the obtained critical exponent γ is consistent with the 3D Ising universal exponent 1.25, although there are scattered results obtained for small D. For the sc lattice, the estimated critical exponent γ is $\gamma\simeq 1.24\pm 0.02$, which is within the range of expected 3D Ising universal exponent. We should point out that, owing to the shortness of the present series, the lower accuracy in the estimates of the critical temperature results in the uncertainties in the estimates of the critical exponent γ.

C. Staggered magnetization

The staggered magnetization M^+ is equal to zero in the disordered phase while in the ordered phase it is found self-consistently from the staggered magnetization series of Eq. (25). The staggered magnetization as a function of temperature in the ordered phase ($T<T_N$) is calculated from the divergence of the series $\overline{M^+}$ defined as[14,25]

$$\overline{M^+}=\frac{\sum_{n=0}^{\infty} m_n(x,y,\lambda)\{\beta J\}^n}{M^+-\sum_{n=0}^{\infty} m_n(x,y,\lambda)\{\beta J\}^n}=\sum_{n=1}^{\infty} b_n(x,y,\lambda)\{\beta J\}^n, \tag{30}$$

where $m_0=M_0^+$. For $M^+=0$, the series $\overline{M^+}$ is equivalent to the staggered susceptibility series, namely,

$$\lim_{M^+\rightarrow 0}\sum_{n=1}^{\infty} b_n\{\beta J\}^n=Jz\chi^s. \tag{31}$$

If the self-consistently determined value of M^+ has been chosen then the series $\overline{M^+}$ diverges as the order of the series M^+ goes to infinity. Thus, the series $\overline{M^+}$ is analyzed using the standard ratio and D-logarithmic Padé approximant method to obtain the magnetic phase boundary in the ordered phase.

With the values of D/J and M^+ fixed, the temperature (kT/J) is solved self-consistently from the extrapolation given by

$$\frac{kT_{n,m}}{J}=\mu(n,m)=\frac{1}{n-m}[nr_n-mr_m], \tag{32}$$

where $r_n=b_n(x,y,\lambda)/b_{n-1}(x,y,\lambda)$. The major source of uncertainty in each estimate of M is the uncertainty in the estimation of temperature kT/J.

In Fig. 3 we show the staggered magnetization M^+ as a function of temperature T of isotropic Heisenberg antiferromagnetic model ($D/J=0$ and $\lambda=1$) for the bcc lattice. In this plot the solid line is drawn through the points obtained from the average of four extrapolations $\mu(5,3)$, $\mu(5,4)$, $\mu(6,4)$, and $\mu(6,5)$. The extrapolation shows good convergence in the sense that each extrapolation value differs from the average value by less than 2% except in the low-temperature region and near the Néel temperature region. The magnetic phase boundary M^+ vs T is also estimated from the D-logarithmic Padé approximants to the staggered magnetization series of Eq. (30) with the fixed values of M^+ for $D/J=0$. The results of $[\frac{2}{2}]$, $[\frac{2}{3}]$, and $[\frac{3}{2}]$ Padé approximants are also plotted in Fig. 3. It is clear from Fig. 3 that the magnetic phase boundary estimated from the D-logarithmic Padé approximants analysis is consistent with that obtained from the ratio analysis in a wide range of temperatures. The predictions of spin-wave theory[26,27] are also shown for comparison. It should be noted that the phase boundary estimated from the series approaches the asymptotic curve which is predicted by spin-wave theory. In the low-temperature region, $kT/J<1.2$, the convergence of the series is slow. The magnetic phase boundary M^+ vs T plot of the isotropic Heisenberg antiferromagnetic model for the sc lattice is shown in Fig. 4. Compared with the bcc lattice, the Padé approximants of isotropic Heisenberg antiferromagnetic model for the sc lattice are less well converged. For the sc lattice higher-order terms are needed to locate the phase boundary more accurately.

In order to estimate the magnetic phase boundary of easy-axis anisotropic Heisenberg antiferromagnetic system, we follow the same procedure as for the isotropic Heisenberg antiferromagnetic model given above. In Fig. 5 we show the staggered magnetization M^+ as a function of temperature T of easy-axis Heisenberg antiferromagnetic Heisenberg antiferromagnetic model for the bcc lattice for $D/J=0.5$, 2.5, and 10.0. In this plot the solid line is drawn through the points obtained from the average of the values given by the four successive approximants. For the range $0.2<M^+<0.9$, the resulting magnetic phase boundary is reliable within 1%. The results of the D-logarithmic Padé approximants are also plotted in Fig. 5. The magnetic phase boundary estimated from the D-logarithmic Padé approximants analysis is consistent with that obtained from the ratio analysis except in the low-temperature region and near the Néel temperature region. For small D the results of the D-logarithmic Padé approximants are scattered in the vicinity of Néel temperature where the thermal fluctuations are large. In addition, the convergence of the series expansion is slow in the low-

TABLE VI. Estimates of critical exponent γ's from the Padé approximant to $-(\beta J-\beta_N J)[d/d(\beta J)]\ln \chi^s$ at the critical point $\beta_N J=J/(kT_N)$ for the sc lattice.

D/J	kT_N/J	$M\backslash L$	2	3	4	5
		2	1.275	1.276	1.275	1.275
1.0	3.166	3	1.275	1.275	1.275	
		4	1.276	1.275		
		5	1.275			
		2	1.247	1.248	1.247	1.248
2.0	3.441	3	1.247	1.247	1.247	
		4	1.247	1.247		
		5	1.248			
		2	1.238	1.239	1.239	1.239
3.0	3.647	3	1.238	1.239	1.239	
		4	1.239	1.240		
		5	1.239			
		2	1.233	1.233	1.233	1.232
4.0	3.812	3	1.233	1.233	1.235	
		4	1.233	1.233		
		5	1.232			
		2	1.232	1.232	1.232	1.230
5.0	3.944	3	1.232	1.232	1.232	
		4	1.232	1.232		
		5	1.230			
		2	1.231	1.233	1.231	1.229
6.0	4.053	3	1.231	1.231	1.232	
		4	1.231	1.231		
		5	1.229			
		2	1.231	1.232	1.232	1.229
7.0	4.142	3	1.231	1.232	1.232	
		4	1.232	1.231		
		5	1.228			
		2	1.232	1.232	1.232	1.229
8.0	4.216	3	1.232	1.232	1.232	
		4	1.232	1.232		
		5	1.229			
		2	1.234	1.234	1.234	1.231
9.0	4.276	3	1.234	1.234	1.234	
		4	1.234	1.234		
		5	1.231			
		2	1.236	1.236	1.236	1.234
10.0	4.325	3	1.236	1.236	1.236	
		4	1.237	1.236		
		5	1.233			

temperature region for small D. The corresponding Ising antiferromagnetic model and mean-field results are also plotted for comparison. For easy-axis Ising antiferromagnetic model, the staggered magnetization series is well converged. Similarly, we show the magnetic phase boundary M^+ vs T plot of the easy-axis Heisenberg antiferromagnetic model for the sc lattice in Fig. 6 for $D/J=0.5$, 2.5, and 10.0.

In the easy-axis isotropic Heisenberg antiferromagnetic system, both the quantum and thermal spin fluctuations play an important role in determining the magnetic ordering. However, both spin fluctuations are suppressed due to the easy-axis anisotropy. Furthermore, the quantum spin fluctuation effect is reduced in spin-1 system and is known to be crucial to determining the magnetic properties of systems in the low-temperature $T\rightarrow 0$ limit. For the small energy gap D, where both spin fluctuations arising from the transverse exchange interaction are dominant, we see that the staggered magnetization is reduced from that of the Ising system. It will be noted that for small D the phase boundary appears to reach the saturation staggered magnetization which is reduced from that of the Ising system by quantum spin fluctuations. The effect of quantum fluctuations is more obvious in sc lattice. The disordering effect of spin fluctuations from the transverse exchange interaction is suppressed as the energy gap D becomes larger. Therefore, for large D the staggered magnetization of the Heisenberg antiferromagnetic system approaches that of the Ising model.

IV. SUMMARY AND CONCLUSIONS

In conclusion, we have studied the magnetic properties of the spin-1 Heisenberg and Ising antiferromagnet with easy-axis single-ion anisotropy using the linked-cluster expansion in both ordered and disordered phases. The staggered susceptibility up to the seventh-order series and the staggered magnetization up to the sixth-order series for the bcc and sc lattices are obtained. The series are analyzed by using both the ratio method and the D-logarithmic Padé approximants.

With the seventh-order series of the staggered susceptibility in the disordered phase, we obtain the dependence of Néel temperature on easy-axis anisotropy of Heisenberg and Ising antiferromagnetic models for the bcc and sc lattices accurately. In addition, the estimated critical exponents of Heisenberg antiferromagnetic model with easy-axis single-ion anisotropy for the sc and bcc lattices are generally consistent with the 3D Ising universal exponent 1.25, although there are scattered results obtained for small D.

We have also shown the magnetic phase boundary in the ordered phase of spin-1 Heisenberg and Ising antiferromagnetic model with easy-axis single-ion anisotropy for the bcc and sc lattices. The convergence of the staggered magnetization series is well for the range $0.2<M^+<0.9$ and becomes better as easy-axis anisotropy increases or the coordination number increases. However, the convergence of the staggered magnetization series is usually slow in the low-temperature region and near the Néel temperature region. Hence, a longer series is needed to locate the phase boundary with greater precision in these regions. The present calculation also shows that the correlation of quantum and thermal fluctuations plays a major role in determining the critical behavior of the system.

ACKNOWLEDGMENTS

This research was supported by Chang Gung University of the Republic of China under Grant No. UMRPD570061. The computations were done on the Compaq DS 20E and IBM P690 of the National Center for High-Performance Computing (NCHC). I wish to thank NCHC for its support.

[1] *Crystalline Electric Field and Structural Effect in f-Electron Systems*, edited by J. E. Crow, R. P. Gruertin, and T. W. Mihalisin (Plenum, New York, 1980).
[2] *Magnetic properties of Layered Transition Metal Compounds*, edited by L. J. de Jongh (Kluwer, Dordrecht, 1990).
[3] W. Knafo, C. Meingast, K. Grube, S. Drobnik, P. Popovich, P. Schweiss, P. Adelmann, T. Wolf, and H. v. Lohneysen, Phys. Rev. Lett. **99**, 137206 (2007).
[4] Y. L. Wang, D. Yang, and M. R. H. Khajehpour, J. Appl. Phys. **42**, 1418 (1971).
[5] I. J. Junger, D. Ihle, and J. Richter, Phys. Rev. B **72**, 064454 (2005).
[6] M. Takahashi, Phys. Rev. B **50**, 3045 (1994).
[7] T. Roscilde and S. Haas, Phys. Rev. Lett. **99**, 047205 (2007).
[8] S. Yamamoto and S. Miyashita, Phys. Rev. B **50**, 6277 (1994).
[9] J. F. Devlin, Phys. Rev. B **4**, 136 (1971).
[10] J. Oitmaa and C. J. Hamer, Phys. Rev. B **77**, 224435 (2008), and references therein.
[11] O. Rojas, S. M. de Souza, E. V. Corrêa Silva, and M. T. Thomaz, Phys. Rev. B **72**, 172414 (2005), and references therein.
[12] Han-Ting Wang and Yupeng Wang, Phys. Rev. B **71**, 104429 (2005).
[13] W. H. Wong, C. F. Lo, and Y. L. Wang, Phys. Rev. B **50**, 6126 (1994).
[14] K. K. Pan, Phys. Lett. A **271**, 291 (2000); Phys. Rev. B **59**, 1168 (1999); Phys. Lett. A **244**, 169 (1998).
[15] C. Wentworth and Y. L. Wang, Phys. Rev. B **36**, 8687 (1987); Y. L. Wang, C. Wentworth, and B. Westwanski, *ibid.* **32**, 1805 (1985).
[16] K. K. Pan and Y. L. Wang, Phys. Rev. B **51**, 3610 (1995); Phys. Lett. A **178**, 325 (1993).
[17] D. S. Gaunt and A. J. Guttman, in *Phase Transitions and Critical Phenomena*, edited by C. Domb and M. S. Green (Academic, New York, 1974), Vol. 3.
[18] A. A. Abrikosov, L. P. Gor'kov, and I. Ye. Dzyaloshinsky, *Quantum Field Theoretical Methods in Statistical Physics* (Pergamon, New York, 1965).
[19] M. Wortis, in *Phase Transitions and Critical Phenomena*, edited by C. Domb and M. S. Green (Academic, New York, 1974).
[20] F. Lee and H. H. Chen, Phys. Rev. B **30**, 2724 (1984).
[21] R. Kubo, J. Phys. Soc. Jpn. **17**, 1100 (1962).
[22] K. K. Pan, Phys. Rev. B **71**, 134524 (2005).

[23] G. S. Rushbrooke and P. J. Wood, Mol. Phys. **6**, 409 (1963); G. S. Rushbrooke, G. A. Baker, and P. J. Wood, in *Phase Transitions and Critical Phenomena*, edited by C. Domb and M. S. Green (Academic, New York, 1974).

[24] G. A. Baker, Jr., H. E. Gilbert, J. Eve, and G. S. Rushbrooke, Phys. Rev. **164**, 800 (1967).

[25] D. S. Gaunt and G. A. Baker, Jr., Phys. Rev. B **1**, 1184 (1970); Y. L. Wang and F. Lee, *ibid.* **29**, 5156 (1984).

[26] P. W. Anderson, Phys. Rev. **86**, 694 (1952); R. Kubo, *ibid.* **87**, 568 (1952); T. Oguchi, *ibid.* **117**, 117 (1960).

[27] J. Oitmaa, C. J. Hamer, and Zheng Weihong, Phys. Rev. B **50**, 3877 (1994).